Aeroacoustics Conferences
30 May - 1 June, 2016, Lyon, France
22nd AIAA/CEAS Aeroacoustics Conference

CrossMark
click for updates

Effect of Nozzle-Plate Distance on Acoustic Phenomena from Supersonic Impinging Jet

Masahito Akamine[1] and Koji Okamoto[2]
The University of Tokyo, Kashiwa, Chiba, 277-8561, Japan

Kent L. Gee[3] and Tracianne B. Neilsen[4]
Brigham Young University, Provo, UT, 84602

Susumu Teramoto[5] and Takeo Okunuki[6]
The University of Tokyo, Bunkyo, Tokyo, 113-8656, Japan

and

Seiji Tsutsumi[7]
Japan Aerospace Exploration Agency, Sagamihara, Kanagawa, 252-5210, Japan

Downloaded by UNIVERSITY OF TOKYO on June 5, 2016 | http://arc.aiaa.org | DOI: 10.2514/6.2016-2930

This study investigates the effect of nozzle-plate distance on the acoustic phenomena from a correctly expanded supersonic jet impinging on an inclined flat plate. In the authors' previous study, the overall sound-pressure-level (OASPL) in the direction almost perpendicular to the plate from the impingement region became highest when the nozzle-plate distance was $15D$ (D, the nozzle exit diameter), although its mechanism was not clarified. In this study, the results of the sound-pressure-level measurement, conditional sampling analysis, and ray tracing of the acoustic intensity vectors are combined to discuss the phenomenon above more in detail. The result shows that the OASPL increase in the $15D$ case is mainly due to the Mach wave, which is generated from the free-jet region and reflects on the flat plate on the bottom side of the jet.

I. Introduction

Suppression of the acoustic vibration is an important factor for the development of a next-generation launch vehicle. One of the sources of vibration is considered to be the acoustic waves from a supersonic exhaust plume. In addition, jet impingement affects the acoustic phenomenon seriously. For example, Panda[1] reported that the location of noise source region in the impinging jet case is different from that of the free jet case at a model-scale test. Moreover, the numerical study by Tsutsumi et al.[2] showed that a slight change in the deflector shape yields large difference in the characteristics of acoustic waves from the impinging exhaust jet. To understand these phenomena, it is necessary to investigate the sound generation mechanisms from a supersonic impinging jet.

A supersonic impinging jet has been studied by many researchers in terms of a flow field[3,4], shock structures[5-8], and the impingement tone[9-14, 29-31]. In addition, a broadband acoustic phenomenon associated with impingement has been recently discussed numerically by Nonomura et al.[15,16] and Tsutsumi et al.[17,18] and experimentally by Worden et al.[19,20] and Akamine et al.[21] These numerical simulations[15-18] and experiment[21] showed that two types of the acoustic waves are generated from a ideally expanded jet impinging on an inclined flat plate. Figure 1a shows a schlieren image, which was discussed in Ref. 21, and Fig. 1b is its schematic view. One of the acoustic waves is considered to be the

[1] Ph.D. Candidate, Dept. of Advanced Energy, Graduate School of Frontier Sciences, AIAA Member.
[2] Associate Professor, Dept. of Advanced Energy, Graduate School of Frontier Sciences, AIAA Member.
[3] Associate Professor, Dept. of Physics and Astronomy, N283 ESC, AIAA Member.
[4] Part-Time Assistant Professor, Dept. of Physics and Astronomy, N283 ESC, AIAA Member.
[5] Associate Professor, Dept. of Aeronautics and Astronautics, Graduate School of Engineering, AIAA Senior Member.
[6] Senior Engineer, Dept. of Aeronautics and Astronautics, Graduate School of Engineering.
[7] Associate Senior Researcher, Aerospace Research and Development Directorate, Research Unit III, AIAA Member.

Copyright © 2016 by the authors. Published by the American Institute of Aeronautics and Astronautics, Inc., with permission.

Mach wave from a free-jet region (the flow between the nozzle exit and impingement region) and wall-jet region (the flow along the plate surface after impingement). The Mach wave is generated due to a supersonic convection of the large turbulent structures in the jet shear layer as explained by Tam.[22] The other is an acoustic wave propagating in approximately 75° from the plate surface. An important point is that the source region of this acoustic wave is located around the shock structures in the impingement region such as a plate shock (i.e., stand-off shock) and series of shock waves on the plate surface, which will be due to the rapid expansion of the jet diameter as discussed by Carling and Hunt.[5]

Akamine et al.[23] also investigated this acoustic phenomenon in the cases of longer nozzle-plate distances. They found that the acoustic wave propagating at 75° from the plate surface became more intense in the longer distance case, while the jet Mach number just before the impingement became lower, but its mechanisms could not be clarified. Therefore, the objective of this study is to explain this phenomenon by combining the results of the sound-pressure-level (SPL) measurement, conditional sampling analysis of visualization movie, and vector acoustic intensity measurement, which have been reported independently in Refs. 23, 24, and 25.

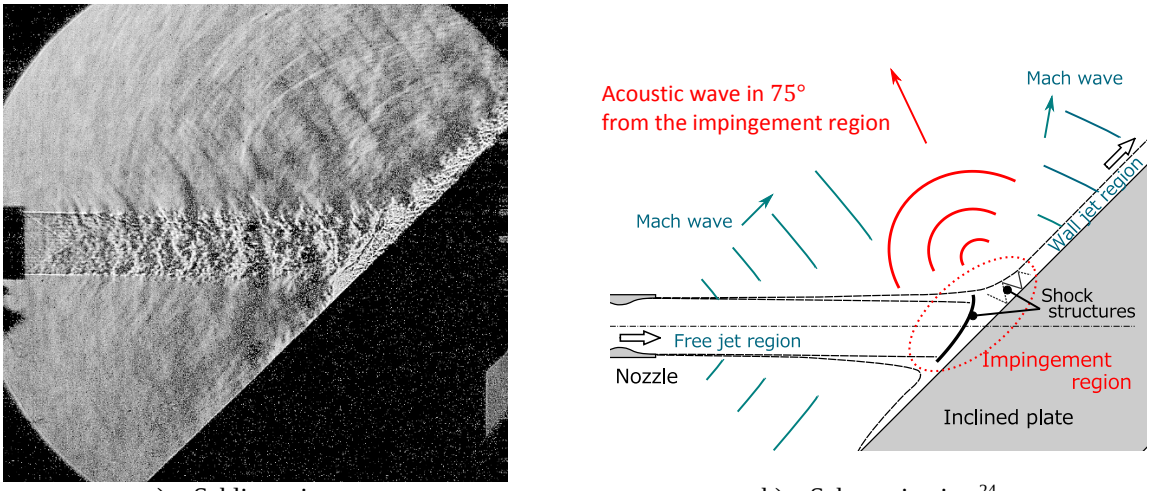

a) Schlieren image b) Schematic view[24]

Figure 1. Acoustic phenomena from supersonic impinging jet.

II. Experimental Methods

A. Jet Facility

The experiment was carried out at the Hypersonic and High-Enthalpy Wind Tunnel at Kashiwa Campus of the University of Tokyo. Table 1 and Fig. 2 show the experimental condition and nomenclature. A Mach 1.8 ideally expanded jet was generated using an axisymmetric convergent-divergent nozzle (exit diameter, $D = 20$ mm). This jet impinged on a 45° inclined flat plate. The nozzle-plate distance ($o - o'$ in Fig. 2) was varied between $5D$ and $25D$. The detailed description of the jet facility, nozzle, and inclined flat plate are found in Ref. 21.

Table 1. Experimental condition.

Jet Mach number	M_j	1.8
Nozzle exit diameter, mm	D	20
Stagnation pressure, MPa		0.585 ± 0.01
Stagnation temperature, K		300
Reynolds number	Re_D	1.5×10^6
Nozzle-plate distance, D		$5 - 25$
Plate angle, deg		45

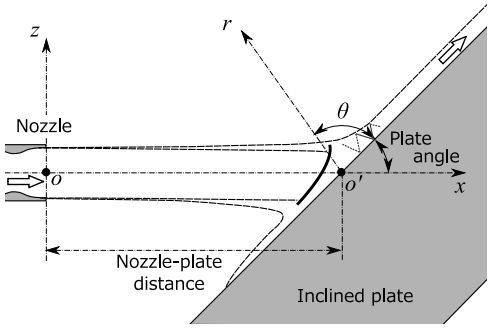

Figure 2. Coordinate system and nomenclature[24].

Downloaded by UNIVERSITY OF TOKYO on June 5, 2016 | http://arc.aiaa.org | DOI: 10.2514/6.2016-2930

B. Sound-Pressure-Level (SPL) Measurement

To observe the acoustic field, the sound-pressure level (SPL) was measured using a single 1/4" free-field microphone (Brüel & Kjær Type 4939) with a two-axes positioning system. The relative location of the measurement points to the inclined flat plate was the same regardless of the nozzle-plate distance. Figure 4 shows the measurement points in the nozzle-plate distance $5D$ case. The signal was acquired using the National Instruments DAQ PCI-6133 and LabView (sampling frequency, 400 kHz; signal length, 1 second). As described in Ref. 21, the narrow-band SPL (or power spectral density) was obtained using the fast Fourier transform and corrected with a microphone free-field response curve (incidence angle 0°) because the microphone pointed at o' of Fig. 2 within 30°. Then, the overall SPL (OASPL) was calculated using the SPLs of $1 - 40$ kHz.

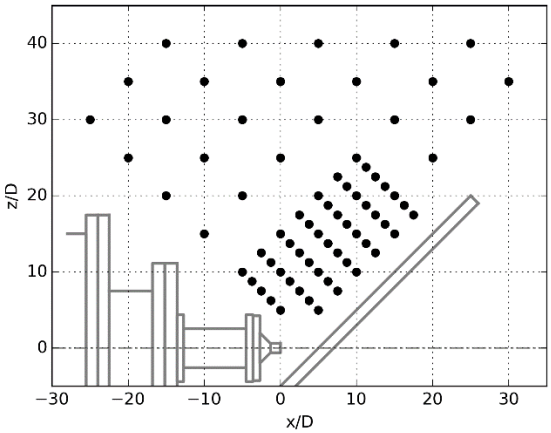

Figure 3. SPL measurement points (Nozzle-plate distance, 5D).

C. Conditional Sampling Analysis of Visualization Movies

To extract phenomena that correlates to the acoustic wave, a conditional sampling analysis was applied to the visualization movies. The detail of this technique was described in Ref. 24. The schlieren visualization movie and trigger signal from a microphone were taken synchronously. The microphone for the trigger signal was set at $r/D = 40, \theta = 75°$ to detect the acoustic wave propagating in 75°. The microphone and data acquisition system were the same as those in Sec. II. B. The visualization movie was taken using a schlieren optical system, which consists of a mercury lamp, concave mirrors (diameter, 200 mm; focal length, 2 m), knife edge (perpendicular to the jet axis), and a high-speed camera (Photron FASTCAM SA-Z; exposure time, approximately 0.37 μs; frame rate, 100 kHz; movie length, 1 second; resolution, 512×328 pixels).

The procedure of the conditional sampling is as follows. With the continuous wavelet transform of the trigger-microphone signal (Fig. 4a), the absolute value of the wavelet coefficient as a function of time and frequency is obtained (Fig. 4b). The peaks of this map correspond to the intermittent acoustic wave. If the 15 kHz component is chosen, for example, two peaks can be found in Fig. 4b. Because the phase value of these peaks is not constant as shown in Fig. 4c, trigger of these peaks is set at a time when the phase value takes $-\pi$ just before the peak (red arrows in Fig. 4c). Then, the frame at an offset time τ before each trigger is obtained from a visualization movie (Fig. 4d). By averaging these frames, uncorrelated phenomena are cancelled and correlated phenomena are extracted (Fig. 4e). By varying the offset time τ, the movie of the correlated phenomena is extracted.

Downloaded by UNIVERSITY OF TOKYO on June 5, 2016 | http://arc.aiaa.org | DOI: 10.2514/6.2016-2930

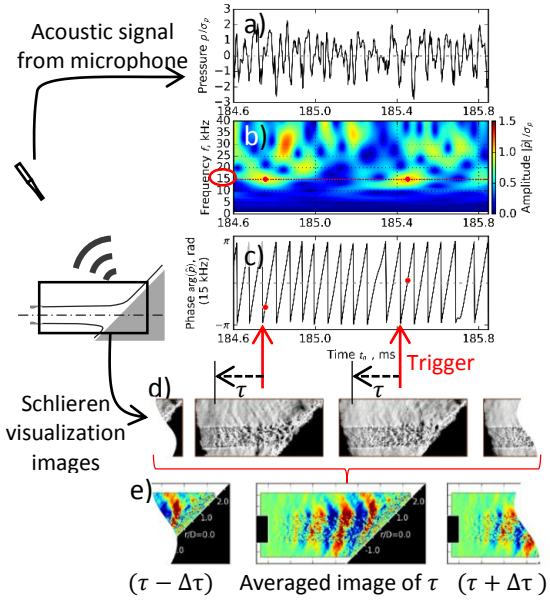

Figure 4. Conditional sampling analysis[24].

D. Vector Acoustic Intensity Measurement

To obtain the intensity level and propagation direction of the acoustic wave simultaneously, the vector acoustic intensity measurement was carried out as described by Gee et al.[25] In this study, the active (radiated) intensity was the focus. To obtain the active intensity, the Phase and Amplitude Gradient Estimator (PAGE) method proposed by Thomas et al.[26] was used. In this method, the active vector intensity of frequency f was formulated with the following equation by Mann and Tichy[27]:

$$\boldsymbol{I} = \frac{1}{\omega\rho_0} P^2 \nabla\phi, \tag{1}$$

where $\omega = 2\pi f$, and ρ_0 is the density of the surrounding atmosphere. P and $\nabla\phi$ are the effective value of pressure magnitude and phase gradient of the complex pressure at frequency f and are calculated using acoustic signals of an intensity probe. The two-dimensional intensity probe consisted of four, parallel-axis 1/4" pressure microphones (G.R.A.S. 46BG) located and the vertices and center of an equilateral triangle, as illustrated in Fig. 5a. As shown in Fig. 5b, four probes were attached on the two-axes positioning system during the experiment. Using these probes, intensity vectors were obtained at the points shown in Fig. 6. The signals were acquired using the National Instruments PXI-4498 (sampling frequency, 204.8 kHz; signal length, 6.1 seconds).

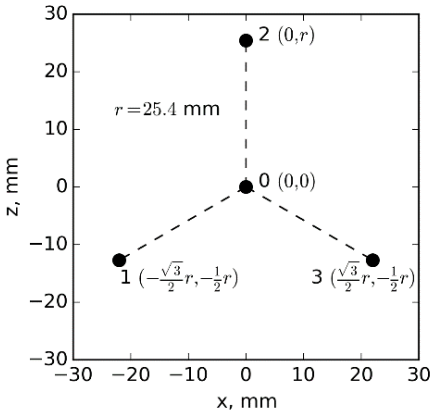

a) Microphone location

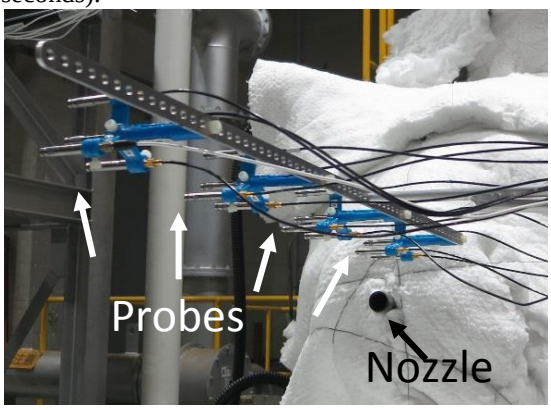

b) Photograph of probes attached to the two-axis positioning system

Figure 5. Two-dimensional intensity probe[28]

Downloaded by UNIVERSITY OF TOKYO on June 5, 2016 | http://arc.aiaa.org | DOI: 10.2514/6.2016-2930

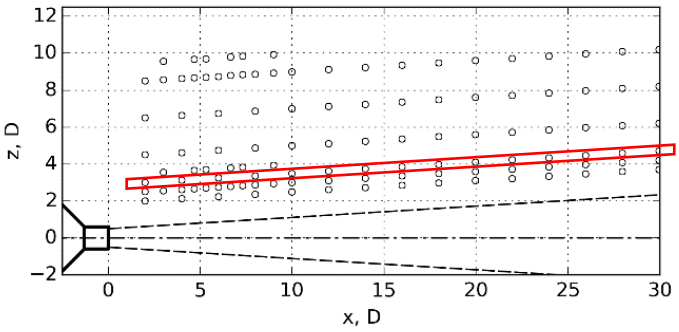

Figure 6. Measurement points of acoustic intensity vectors[28] (red square: measurement points for reflected Mach wave estimation in Sec. III. B).

Downloaded by UNIVERSITY OF TOKYO on June 5, 2016 | http://arc.aiaa.org | DOI: 10.2514/6.2016-2930

III. Results and Discussion

A. Important Results in the Previous Papers

To facilitate the discussion of how these different analyses contribute to the objective of identifying the source of the 75° noise component for impinging plates, the important results in Refs. 21, 23, and 24 are reviewed in this section. Figures 7a and 7b show OASPL distributions in the nozzle-plate distance $5D$ and $15D$ cases, respectively. In both cases, the acoustic wave propagating in the 75° direction (towards B) is observed, as well as the acoustic waves in the direction A, which is considered to be the Mach wave from the wall-jet region (the flow along the plate surface after impingement). Figure 8 shows the OASPL at $r/D = 40, \theta = 75°$ (red point in Fig. 7) for different nozzle-plate distances to observe variation of the OASPL of the acoustic wave in 75° across different measurements. The OASPL is highest in the $15D$ case, as seen in this plot, even though it has some errors.

On the other hand, according to Akamine et al.,[21] the centerline Mach number of the free jet is about 1.8 and 1.3 at $5D$ and $15D$ downstream of the nozzle exit, respectively. This Mach number drop yields the weaker shock structures in the $15D$ case in the impingement region, which is close to the source region of the acoustic wave propagating in the 75° direction. Figure 9 shows the time-averaged wall pressure measured using flush-mounted pressure transducers. The horizontal axis is r for $\theta = 0°$ (along the plate surface) in Fig. 2. As seen in this plot, two pressure peaks due to the shock structures in the $5D$ case do not appear in the $15D$ case. An important conclusion from this study is that there is no correlation found between the strength of the shock structures and the OASPL at $r/D = 40, \theta = 75°$, even though the apparent source location is close to the shock structures. To discuss this OASPL increase in the following sections, the two cases of the nozzle-plate distances of $5D$ and $15D$ are selected because, in the $5D$ case, the nozzle-plate distance is shortest and effects of the jet impingement are large in this experiment and, in the $15D$ case, the OASPL is highest.

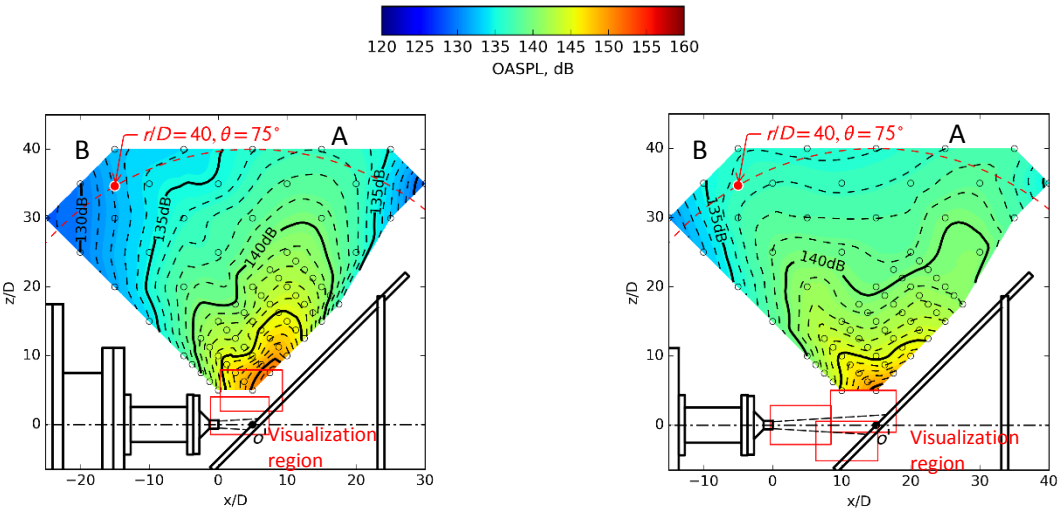

a) Nozzle-plate distance, 5D b) Nozzle-plate distance, 15D

Figure 7. OASPL distribution[24].

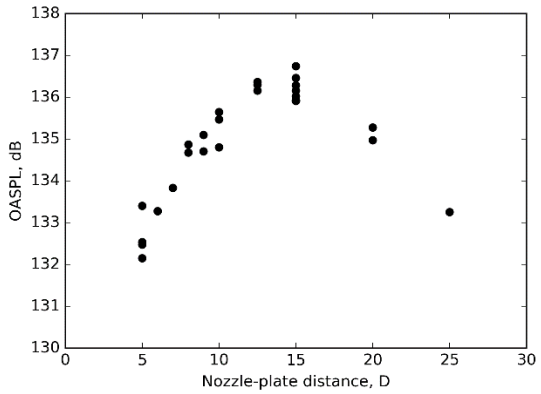

Figure 8. OASPL at $r/D = 40, \theta = 75°$ as a function of the nozzle-plate distance[24].

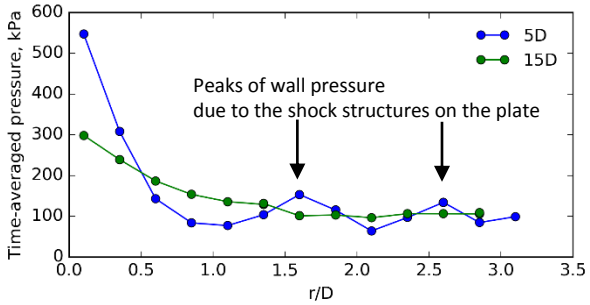

Figure 9. Wall pressure distribution[23].

The conditional sampling analysis by Akamine et al.[24] shed a new light on the cause of the OASPL increase. They extracted phenomena that correlated to the acoustic wave at $r/D = 40, \theta = 75°$ from the schlieren visualization movies around the source region. Figures 10a and 10b show the extracted images in the $5D$ and $15D$ cases, respectively. To compare these two cases, the extractions were carried out using 300 triggers at 13 ± 1 kHz, which is the peak frequency at $r/D = 40, \theta = 75°$ in the $5D$ case. The Mach wave from the free-jet region (the flow between the nozzle exit and impingement region) is extracted in both cases but their features are different. In the $5D$ case (Fig. 10a), the Mach wave appears on both the upper and lower sides of the jet, while that in the $15D$ case (Fig. 10b) appears only on the lower side. This result suggests that the Mach wave from the free-jet region may play an important role on the OASPL increase at $r/D = 40, \theta = 75°$ but its process will be different. One of the possible processes is a simple reflection of the Mach wave on the flat plate.

Downloaded by UNIVERSITY OF TOKYO on June 5, 2016 | http://arc.aiaa.org | DOI: 10.2514/6.2016-2930

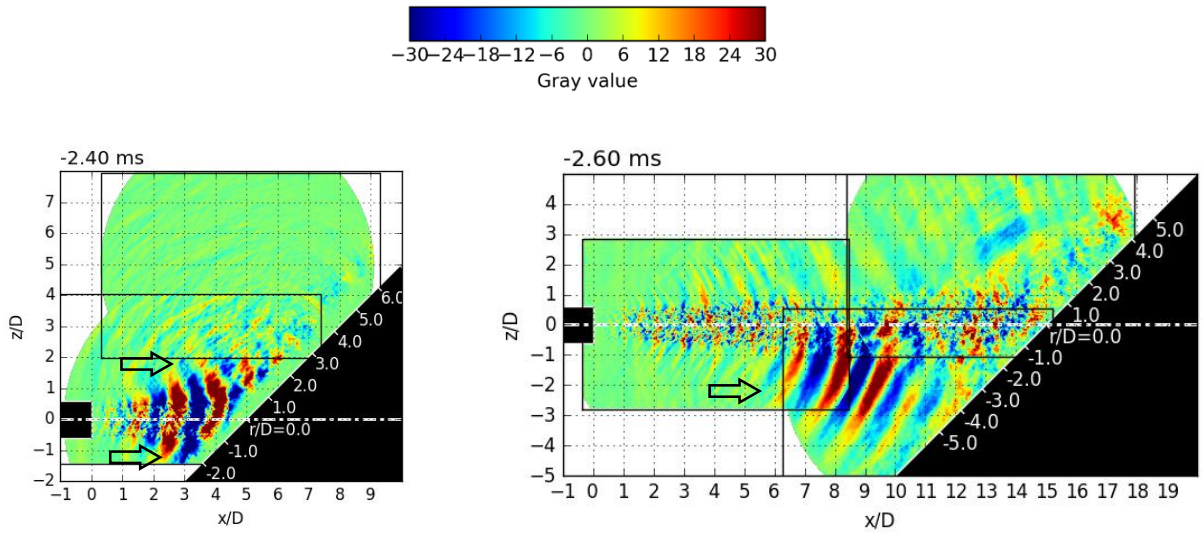

a) Nozzle-plate distance, 5D ($\tau = -2.4$ ms)

b) Nozzle-plate distance, 15D ($\tau = -2.6$ ms)

Figure 10. Mach wave from free-jet region extracted from visualization movies (trigger frequency: 13 kHz; location of trigger microphone: $r/D = 40, \theta = 75°$).

B. Estimation of Propagation Path of Reflected Mach Wave

Evidence for estimating the propagation path of the reflected Mach wave can be found from the acoustic vector intensity measurements. Gee et al.[25] measured the acoustic intensity vectors of the free jet and obtained a map of the intensity level and propagation direction of the acoustic wave for each frequency, similar to the one shown in Fig. 11 for 13 kHz. The color contour and vector direction show the intensity level and propagation direction, respectively. Furthermore, by tracing back these vectors to the jet centerline, they estimated the location of the source region.

In this study, by using this ray-tracing technique, the propagation region of the Mach wave reflected by the inclined flat plate is estimated as follows. For the measurement locations along the blue line in Fig. 11, the intensity vectors at these locations with intensity level over 115 dB are selected as those dominated by the Mach wave. These intensity vectors are shown on the blue lines in Fig. 12. Note that the vectors beneath the jet are obtained from those measured above the jet, by assuming that the acoustic field is axisymmetric. By assuming the source region is located along the jet boundary, the ray tracing each of the high level intensity vectors leads to an estimated source location for the Mach waves from the free jet case According to the visualization movies, the jet boundary exists along the line from the nozzle with approximately 3.5° to the jet axis, shown as light gray dashed lines in Fig. 11 and 12. The tracing paths for the free jet case are shown as the red or green dashed lines in Fig. 12. The vectors between the nozzle exit and plate surface are selected. Assuming specular reflection of the selected tracing paths by the inclined flat plate, the propagation paths of the reflected Mach wave are obtained as the red and green solid lines in Fig. 12. Note that the diffraction is not considered in this ray tracing.

This ray-tracing of acoustic vector intensity leads to insights into the variation of Mach wave radiation with the nozzle-plate distance. Figure 12a shows that few propagation paths of the reflected Mach wave appear in the $5D$ case. This indicates that the propagation region of the reflected Mach wave will be narrow. On the other hand, Fig. 12b shows that the all propagation paths are reflected by the inclined flat plate. Therefore, the propagation region will be wider than in the $5D$ case.

Downloaded by UNIVERSITY OF TOKYO on June 5, 2016 | http://arc.aiaa.org | DOI: 10.2514/6.2016-2930

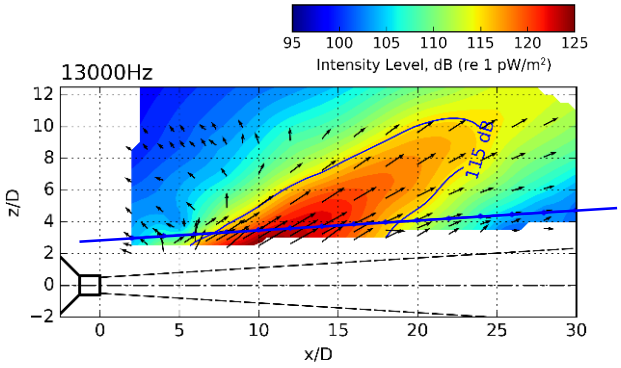

Figure 11. Acoustic intensity vectors (Free jet; frequency, 13 kHz).

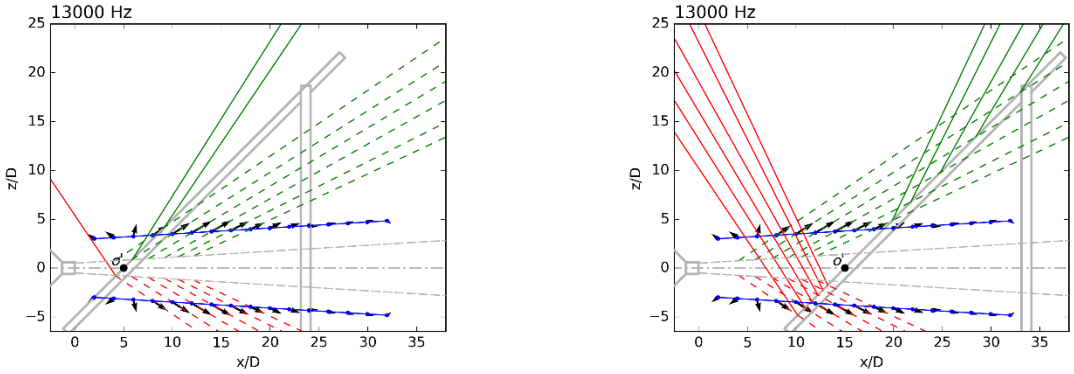

a) Nozzle-plate distance, 5D b) Nozzle-plate distance, 15D

Figure 12. Estimation of reflected Mach wave from the free jet region (frequency, 13 kHz; red or green dashed line, propagation path of the Mach wave from the free jet; red or green solid line, that of the Mach wave reflected by the inclined flat plate).

C. Comparison with Extracted Phenomena from Visualization Movies

This section discusses the differences of the extracted phenomena from the visualization movies between the cases of the nozzle-plate distance $5D$ and $15D$, by combining the propagation region of the reflected Mach wave estimated in the last section. In Figs. 13 and 14, the propagation paths are drawn on frames of the extracted movies in the $5D$ and $15D$ cases, respectively.

In the $5D$ case, the propagation paths in Fig. 13 indicate that the reflected Mach wave will propagate in two directions: along the inclined flat plate (green solid lines) and almost perpendicular direction to the plate from the lower side ($r/D = -1.0$) of the impingement region(red solid line). On the other hand, the extracted waves in Fig. 13b originate at the upper side of the impingement region around $r/D = 1.0$ and propagate in three directions: along the plate surface, almost perpendicular direction to the plate, and upstream direction. Therefore, although the Mach wave appears in the free jet region in Fig. 13a, the extracted waves in Fig. 13b cannot be regarded only as the reflected Mach wave.

On the other hand, in the $15D$ case in Figs. 14c and 14d, the Wave X propagates in the direction almost perpendicular to the plate from a source region similar to that in the $5D$ case (upper side of the impingement region around $r/D = 1.0$). In addition to this, Figs. 14c and 14d show the Wave Y, which propagates along the estimated propagation paths of the reflected Mach wave (red solid line). This indicates that the Wave Y is the reflected Mach wave. Note that the Mach wave on the upper side of the jet is also extracted in Fig. 14c.

It is summarized that, in the extracted movies, the waves are radiated from the upper side of the impingement region and cannot be regarded only as the reflected Mach wave in the $5D$ case, while both the reflected Mach wave and the wave from the upper side of the impingement region appear in the $15D$ case.

Downloaded by UNIVERSITY OF TOKYO on June 5, 2016 | http://arc.aiaa.org | DOI: 10.2514/6.2016-2930

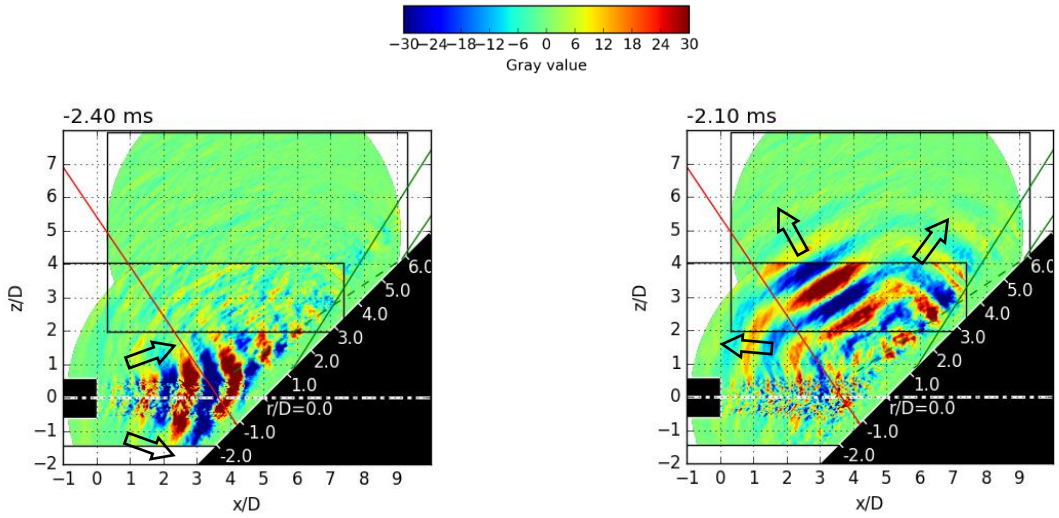

a) $\tau = -2.4$ ms b) $\tau = -2.1$ ms

Figure 13. Comparison between extracted images (trigger frequency, 13 kHz; location of trigger microphone, $r/D = 40, \theta = 75°$) and estimated propagation region of the reflected Mach wave (frequency, 13 kHz) in nozzle-plate distance 5D case.

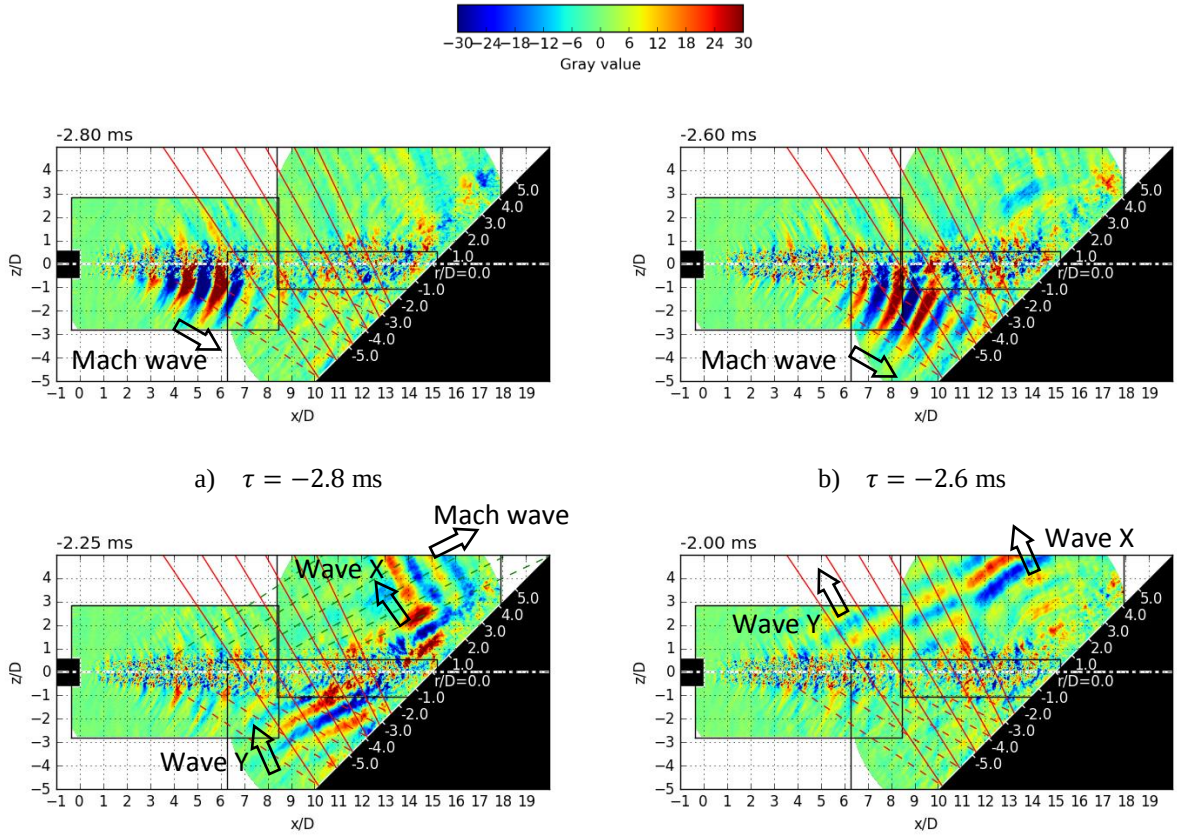

a) $\tau = -2.8$ ms b) $\tau = -2.6$ ms

c) $\tau = -2.25$ ms d) $\tau = -2.0$ ms

Figure 14. Comparison between extracted images (trigger frequency, 13 kHz; location of trigger microphone, $r/D = 40, \theta = 75°$) and estimated propagation region of the reflected Mach wave (frequency, 13 kHz) in nozzle-plate distance 15D case.

Downloaded by UNIVERSITY OF TOKYO on June 5, 2016 | http://arc.aiaa.org | DOI: 10.2514/6.2016-2930

D. Comparison with OASPL Differences

This section discusses contribution of the reflected Mach wave to the OASPL increase at $r/D = 40, \theta = 75°$ in the $15D$ case. By subtracting the OASPL in the $5D$ case from those in the $10D$, $15D$, and $20D$ cases, Figs. 15a, 15b, and 15c are obtained, respectively. Note that the subtraction is performed between the OASPL values at the same location relative to the inclined flat plate. Also, the propagation paths of the reflected Mach wave estimated in Sec III. B. are drawn as the red or green solid lines on these figures.

In all the cases, the propagation paths show the two propagation regions of the reflected Mach wave. In these regions, the OASPL increases by $4 - 6$ dB in the $15D$ and $20D$ cases (Figs. 15b and 15c). Also, in the $10D$ case (Fig. 15a), the OASPL along the red solid line slightly increases. This OASPL increase is considered to be mainly due to the reflected Mach wave. This region almost includes the point at $r/D = 40, \theta = 75°$, which is the measurement point of Fig. 8. On the other hand, in the region that corresponds to the acoustic waves from the upper side of the impingement region (the Wave X in Fig. 14), the OASPL increase cannot be observed, as seen in Fig.15. Therefore, it can be concluded that one of the factors of the OASPL increase at this point is the reflected Mach wave, in particular, in the $15D$ and $20D$ cases.

Besides, the OASPL decreases in the direction A in Figs. 15b and 15c. This region corresponds to the region of the Mach wave from the wall-jet region in the $5D$ case in Fig. 7a. Therefore, it is supposed that the Mach wave from the wall-jet region is weaker because the jet velocity of the wall jet is lower in the $15D$ and $20D$ cases than in the $5D$ case.

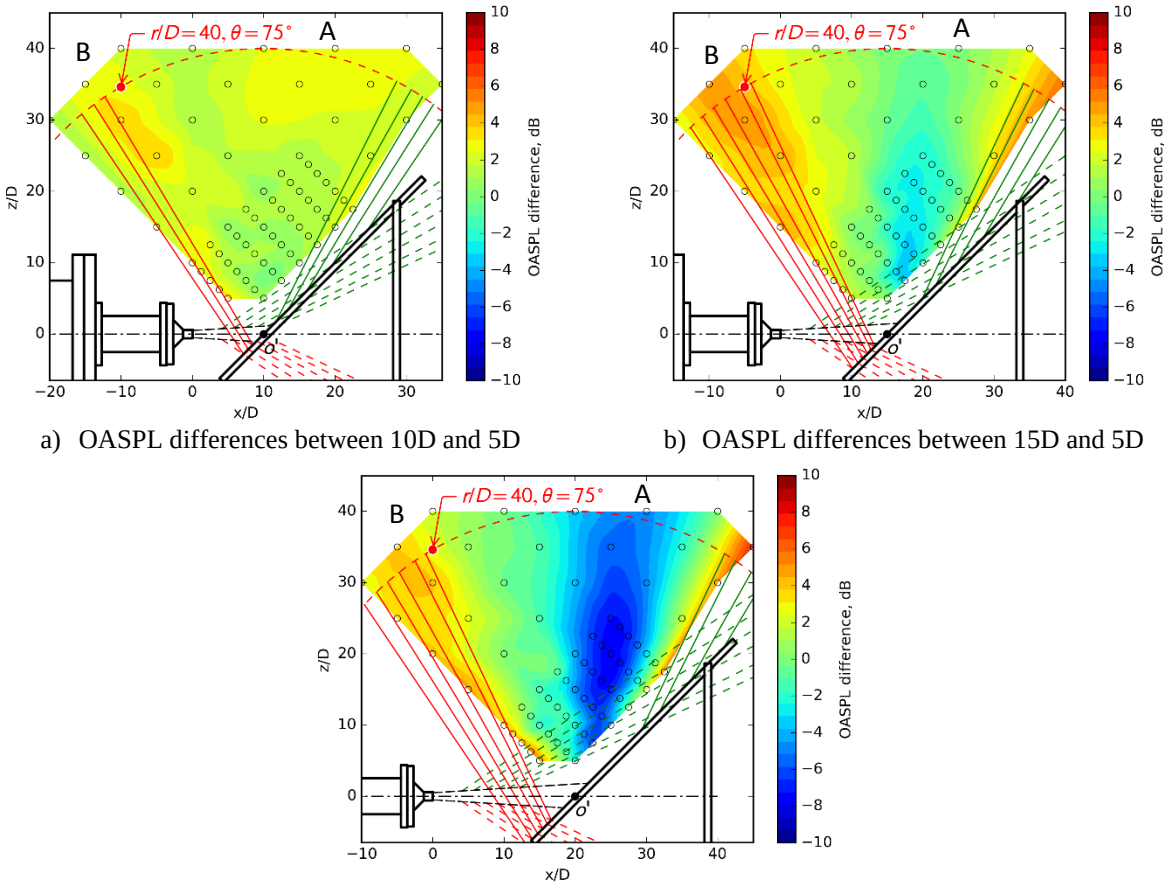

a) OASPL differences between 10D and 5D

b) OASPL differences between 15D and 5D

c) OASPL differences between 20D and 5D

Figure 15. Comparison between OASPL differences and estimated propagation region of the reflected Mach wave.

Downloaded by UNIVERSITY OF TOKYO on June 5, 2016 | http://arc.aiaa.org | DOI: 10.2514/6.2016-2930

IV. Conclusion

This study discussed the effect of the nozzle-plate distance on the acoustic phenomena from the supersonic impinging jet, by combining the results of SPL measurement, conditional sampling analysis of the visualization movies, and ray tracing of the acoustic intensity vectors. The main focus was the reason of the higher OASPL in the direction of $75°$ from the plate surface in the case of the nozzle-plate distance $15D$ than that in the $5D$ case. In the $15D$ case, the wave propagating in the $75°$ direction consists of the Mach wave from the free-jet region reflected by the inclined flat plate and the wave propagating from the upper side of the impingement region. This reflected Mach wave becomes more significant in the $15D$ and $20D$ cases and this is one of the factors of the OASPL increase in the $75°$ direction.

Acknowledgments

A portion of this study was supported by an Invitation Fellowship from the Japan Society for the Promotion of Science. The authors would like to thank Chihiro Konno of the University of Tokyo and Dr. George Kuwabara of Photron Limited. Also, the authors would like to express the appreciation to Darren K. Torrie and Eric B. Whiting of Brigham Young University for their assistance.

References

[1]Panda, J., "Microphone Phased Array to Identify Liftoff Noise Sources in Model-Scale Tests," *Journal of Spacecraft and Rockets*, Vol. 50, No. 5, 2013, pp. 1002-1012.

[2]Tsutsumi, S., Kato, S., Fukuda, K., Takaki, R., and Ui, K., "Effect of Deflector Shape on Acoustic Field of Launch Vehicle at Lift-off," *47th AIAA Aerospace Sciences Meeting*, AIAA Paper 2009-328, 2009.

[3]Donaldson, C. D. and Snedeker, R. S., "A Study of free jet impingement. Part 1. Mean properties of free and impinging jets," *Journal of Fluid Mechanics*, Vol. 45, No. 2, 1971, pp. 281-319.

[4]Henderson, L. F., "Experiments on the Impingement of a Supersonic Jet on a Flat Plate," *Zeitschrift für angewandte Mathematik und Physik ZAMP*, Vol. 17, No. 5, 1966, pp. 553-569.

[5]Carling, J. C. and Hunt, B. L., "The near wall jet of a normally impinging, uniform, axisymmetric, supersonic jet," *Journal of Fluid Mechanics*, Vol. 66, No. 1, 1974, pp. 159-176.

[6]Lamont, P. J. and Hunt, B. L., "The impingement of underexpanded axisymmetric jets on perpendicular and inclined flat plates," *Journal of Fluid Mechanics*, Vol. 100, No. 3, 1980, pp. 471-511.

[7]Nakai, Y., Fujimatsu, N., and Fujii, K., "Experimental Study of Underexpanded Supersonic Jet Impingement on an Inclined Flat Plate," *AIAA Journal*, Vol. 44, No. 11, 2006, pp. 2691-2699.

[8]Goto, Y., Nonomura, T., McIlroy, K., and Fujii, K., "Detailed Analysis of Flat Plate Pressure Peaks Created by Supersonic Jet Impingements," *47th AIAA Aerospace Sciences Meeting*, AIAA Paper 2009-1289, 2009.

[9]Henderson, B., "The connection between sound production and jet structure of the supersonic impinging jet," *The Journal of the Acoustical Society of America*, Vol. 111, No. 2, 2002, pp. 735-747.

[11]Uzun, A., Kumar, R., Hussaini, M. Y., and Alvi, F. S., "Simulation of Tonal Noise Generation by Supersonic Impinging Jets," *AIAA Journal*, Vol. 51, No. 7, 2013, pp. 1593-1611.

[12]Henderson, B., Bridges, J., and Wernet, M., "An experimental study of the oscillatory flow structure of tone-producing supersonic impinging jets," *Journal of Fluid Mechanics*, Vol. 542, 2005, pp. 115-137.

[13]Dauptain, A., Gicquel, L. Y. M., and Moreau, S., "Large Eddy Simulation of Supersonic Impinging Jets," *AIAA Journal*, Vol. 50, No. 7, 2012, pp. 1560-1574.

[14]Risborg, A. and Soria, J., "High-speed optical measurements of an underexpanded supersonic jet impinging on an inclined plate," *28th International Congress on High-Speed Imaging and Photonics*, International Society for Optics and Photonics, 71261F, 2009.

[15]Nonomura, T., Goto, Y., and Fujii, K., "Aeroacoustic waves generated from a supersonic jet impinging on an inclined flat plate," *International Journal of Aeroacoustics*, Vol. 10, No. 4, 2011, pp. 401-426.

[16]Nonomura, T., Honda, H., Nagata, Y., Yamamoto, M., Morizawa, S., Obayashi, S., and Fujii, K., "Plate-Angle Effects on Acoustic Waves from Supersonic Jets Impinging on Inclined Plates," *AIAA Journal*, Vol. 54, No. 3, 2016, pp. 816-827.

[17]Tsutsumi, S., Takaki, R., Nakanishi, Y., Okamoto, K., and Teramoto, S., "Numerical Study on Acoustic Radiation from a Supersonic Jet Impinging to an Inclined Plate," *17th AIAA/CEAS Aeroacoustics Conference*, AIAA Paper 2011-2922, 2011.

[18]Tsutsumi, S., Takaki, R., Nakanishi, Y., Okamoto, K., and Teramoto, S., "Acoustic Generation Mechanism of a Supersonic Jet Impinging on Deflectors," *52nd Aerospace Sciences Meeting*, AIAA Paper 2014-0882, 2014.

[19]Worden, T. J., Gustavsson, J. P. R., Shih, C., and Alvi, F. S., "Acoustic Measurements of High-Temperature Supersonic Impinging Jets in Multiple Configurations," *19th AIAA/CEAS Aeroacoustics Conference*, AIAA Paper 2013-2187, 2013.[18]Tam, 2009.

[20]Worden, T. J., Shih, C., Alvi, F. S., "Supersonic Jet Impingement on a Model-Scale Jet Blast Deflector," *54th AIAA Aerospace Sciences Meeting*, AIAA 2016-1015, 2016.

Downloaded by UNIVERSITY OF TOKYO on June 5, 2016 | http://arc.aiaa.org | DOI: 10.2514/6.2016-2930

[21]Akamine, M., Nakanishi, Y., Okamoto, K., Teramoto, S., Okunuki, T., and Tsutsumi, S., "Acoustic Phenomena from Correctly Expanded Supersonic Jet Impinging on Inclined Plate," *AIAA Journal*, Vol. 53, No. 7, 2015, pp. 2061-2067.

[22]Tam, C. K. W., "Mach Wave Radiation from High-Speed Jets," *AIAA Journal*, Vol. 47, No. 10, 2009, pp. 2440-2448.

[23]Akamine, M., Nakanishi, Y., Okamoto, K., Teramoto, S., Okunuki, T., and Tsutsumi, S., "Experimental Study on Acoustic Phenomena of Supersonic Jet Impinging on Inclined Flat Plate," *52nd Aerospace Sciences Meeting*, AIAA Paper 2014-0879, 2014.

[24]Akamine, M., Okamoto, K., Teramoto, S., Okunuki, T., and Tsutsumi, S., "Conditional Sampling Analysis of Acoustic Phenomena from Supersonic Jet Impinging on Inclined Flat Plate," *30th International Symposium on Space Technology and Science*, 2015.

[25]Gee, K. L., Neilsen, T. B., Whiting, E. B., Torrie, D. K., Akamine, M., Okamoto, S., Teramoto, S., and Tsutsumi, S., "Application of a Phase and Amplitude Gradient Estimator to Intensity-Based Laboratory-Scale Jet Noise Source Characterization," *Berlin Beamforming Conference 2016*, 2016.

[26]Thomas, D. C., Christensen, B. Y., and Gee, K. L., "Phase and amplitude gradient method for the estimation of acoustic vector quantities," *The Journal of the Acoustical Society of America*, Vol. 137, No. 6, 2015, pp. 3366-3376.

[27]Mann, III, J. A. Tichy, J., and Romano, A. J., "Instantaneous and time-averaged energy transfer in acoustic fields," *The Journal of Acoustical Society of America*, Vol. 82, No. 1, 1987, pp. 17-30.

[28]Akamine, M., Okamoto, K., Gee, K. L., Neilsen, T. B., Teramoto, S., Tsutsumi, S., and Okunuki, T., "Comparison of Acoustic Intensity Vectors with SPL and Phase Distributions of Supersonic Jet," *8th Asian Joint Conference on Propulsion and Power*, 2016.

[29]Kumar, R., Wiley, A., Venkatakrishnan, L., and Alvi, F., "Role of coherent structures in supersonic impinging jets," *Physics of Fluids*, Vol. 25, No. 7, 2013, 076101.

[30]Davis, T., Edstrand, A., Alvi, F., Cattafesta, L., Yorita, D., and Asai, K., "Investigation of impinging jet resonant modes using unsteady pressure-sensitive paint measurements," *Experiments in Fluids*, Vol. 56, No. 5, 2015.

[31]Weightman, J., Amili, O., Honnery, D., Edgington-Mitchell, D., and Soria, J., "Effects of Nozzle Lip Thickness on the Global Modes of an Impinging Supersonic Jet," *7th Australian Conference on Laser Diagnostics in Fluid Mechanics and Combustion*, 2015.

Downloaded by UNIVERSITY OF TOKYO on June 5, 2016 | http://arc.aiaa.org | DOI: 10.2514/6.2016-2930